

## Configuration Transition in a Nematic Liquid Crystal Confined to a Small Spherical Cavity

John H. Erdmann, Slobodan Žumer,<sup>(a)</sup> and J. William Doane

*Liquid Crystal Institute and Department of Physics, Kent State University, Kent, Ohio 44242*

(Received 18 August 1989)

The director-field configuration of a nematic liquid crystal confined to a spherical cavity within a urethane polymer is observed to transform from a radial- to axial-type structure as the radius of the cavity, temperature, or strength of an applied electric field are varied. The phase diagram, anchoring strength at the droplet wall, and a value of the reduced field inside the droplet are determined for different polymer/liquid-crystal interfaces.

PACS numbers: 64.70.Md, 61.30.Gd, 68.10.Cr, 78.20.Jq

When a nematic liquid crystal is confined to a small cavity, a variety of unusual effects are introduced as a result of the interplay between the ordering interactions at the surface of the cavity wall and the elastic deformation energies of the liquid crystal inside the cavity.<sup>1-10</sup> The most observable are changes in the nature of the nematic-isotropic transition,<sup>8-11</sup> the specific director configuration inside the cavity,<sup>1-5,7,10</sup> and the variable angle at which the elongated molecule is anchored at the cavity wall.<sup>6-10</sup> In this paper, we report the first study of the latter two effects where a well-defined transition occurs between two possible configurations of the director field inside a spherical cavity with a simultaneous change in the distribution of anchoring angles at the surface.

The studies reported here were motivated by the fact

that in studying polymer-dispersed liquid crystals<sup>12</sup> (PDLC) one rarely observes the radial configuration illustrated in Fig. 1 for nematic droplets, and when such a configuration is observed it is usually in a large droplet. Radial configurations were first reported in large droplets dispersed in glycerol,<sup>3,6</sup> and have been investigated theoretically by a number of workers.<sup>1,10</sup> Suspecting that the surface may be the reason for their rare occurrence, we began to explore, first theoretically, the role of anchoring in a spherical cavity. Limiting our treatment to supramicron droplets, nematic ordering can be assumed uniaxial and be defined by a nematic director  $\mathbf{n}$  and a positionally independent order parameter  $S$ .<sup>9,10</sup> We thus express the total free energy of the confined nematic as

$$F = \frac{1}{2} \int [K_{11}(\text{div } \mathbf{n})^2 + K_{22}(\mathbf{n} \cdot \text{rot } \mathbf{n})^2 + K_{33}(\mathbf{n} \times \text{rot } \mathbf{n})^2] dV - \frac{1}{2} \int \epsilon_0 \Delta \epsilon (\mathbf{E}' \cdot \mathbf{n})^2 dV + \frac{1}{2} \int W_0 \sin^2(\theta - \theta_0) dA. \quad (1)$$

The first three terms in Eq. (1) are the usual contributions of splay, twist, and bend deformations to the free energy, where  $K_{ii}$  are the appropriate elastic constants proportional to  $S^2$ .<sup>13</sup> The fourth term is present when there is an applied field,  $\mathbf{E}$ , and  $\mathbf{E}'$  is the local field inside the droplet and  $\Delta \epsilon$  is the anisotropy of the dielectric constant. The final term is the contribution of the surface where  $W_0$  is the surface anchoring strength, and  $\theta_0$  and  $\theta$  are the preferred and actual anchoring angles, respectively.<sup>14</sup> Other contributions to the free energy, such as the saddle-splay term ( $K_{22}$  and  $K_{24}$ ) and the mixed splay-bend term ( $K_{13}$ ), can be reduced to surface terms and are neglected here. The effects of these additional surface terms are discussed later, but will not affect the qualitative results presented in this Letter.

For the case where the molecules prefer to be anchored perpendicular to the surface and in the absence of an applied field, the minimization of Eq. (1) yields the total free energy of a droplet to be  $8\pi K_{11}R$ .<sup>1</sup> The anchoring strength does not appear in the expression since the molecules are normally oriented at all points on the surface. An alternate structure for perpendicular anchoring is the axial configuration also illustrated in Fig.

1. The free energy for this structure contains both the elastic and surface terms, and is found to be a function of the ratio  $R/d_e$ , where  $R$  is the radius of the cavity and  $d_e = K/W_0$  is the surface extrapolation length.<sup>13</sup> The constant  $K = (K_{11} + K_{33})/2$  is an average elastic constant for the axial structure. In this case the minimization of Eq. (1) is performed numerically, yielding the result that the equatorial defect line which makes the axial structure unstable in the strong-anchoring<sup>4</sup> case is no longer present under weak anchoring and that with a decreasing  $R/d_e$  ratio the structure becomes more and more aligned, as illustrated in Fig. 1. Furthermore, when the total free energy is compared to the radial case, the axial configuration becomes the more stable one when  $R/d_e < 18.2$ .

We observed this transition in a dispersion of nematic droplets in a polyurethane matrix. The dispersion was prepared by phase separating a mixture of nematic material E7 (EM Chemicals) and parts  $A$  (isocyanate prepolymer) and  $B$  (polyol blended curing agent) of polyurethane TU50A (Conap) in a weight ratio of  $y:1:x$  where the concentration of part  $B$ ,  $x$ , was adjusted be-

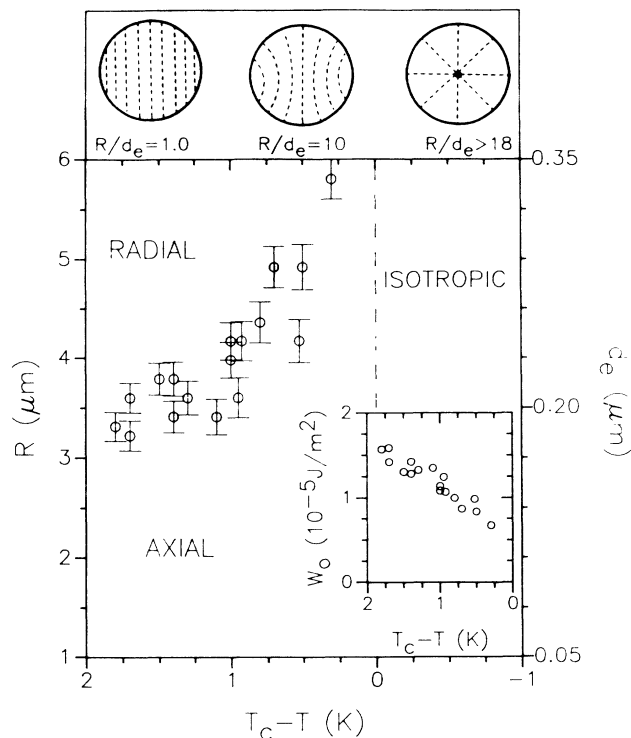


FIG. 1. Transition temperatures for the radial to axial configuration for a droplet of radius  $R$  in a sample with E7, part A, and part B of TU50A mixed in a weight ratio of 0.94:1:1.01. The corresponding extrapolation length,  $d_e$ , is calculated assuming a transition occurs at  $R/d_e = 18.2$ . Inset: The calculated anchoring strengths,  $W_0$ , as a function of temperature. Simulations of the radial and axial configurations are shown above the figure.

tween 1.0 and 1.4 to obtain different polymer/liquid-crystal interfaces, and the concentration of E7,  $y$ , was varied between 0.94 and 1.10 so that all samples would have a liquid-crystal concentration of 32% by weight. We discovered that in order to obtain radial droplets it was necessary that  $x$  be greater than 1, independent of the actual liquid-crystal concentration, although the amount of liquid crystal must be nearly one-third of the total weight for the droplets to form. The phase-separated E7 in the droplets was found to be heavily doped with unreacted polyols from part B of the TU50A, causing the actual nematic-to-isotropic transition temperature,  $T_c = 303$  K, to be reduced 30 K below the value for purified E7. The values of the material constants of our E7 droplet are thus rescaled according to this transition-temperature shift. The polymer is also heavily plasticized with E7, making it quite soft.

The director configuration was monitored by observing droplet texture under a polarizing microscope.<sup>3,6</sup> Figure 1 shows the transition temperatures for a droplet of radius  $R$  to experience a configuration transition from the radial to the axial structure as the temperature is increased in samples with a polymer matrix in which  $B/A$

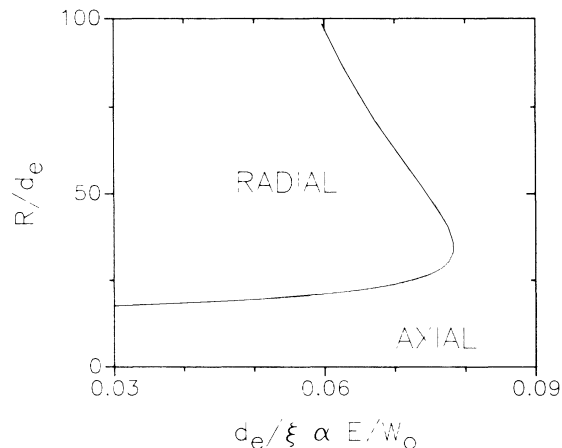


FIG. 2. Calculated regions of stability for the radial and axial configurations. The type of configuration is governed by the droplet radius  $R$ , the surface extrapolation length  $d_e$ , and the effects of an electric field  $E$ , as described by the value of the electric coherence length  $\xi$ .

$= 1.01$ . The corresponding surface extrapolation length which was determined by assuming a configuration transition at  $R/d_e = 18.2$  is also shown in Fig. 1. For this sample, no droplets with the radial configuration were observed below  $R = 2.5$   $\mu\text{m}$  at  $T = 298$  K, corresponding to an extrapolation length  $d_e$  of about 0.14  $\mu\text{m}$ . This yields a value of  $3.3 \times 10^{-5}$  J/m<sup>2</sup> for the anchoring strength  $W_0$ , which was determined using the average value of the  $K_{11}$  and  $K_{33}$  elastic constants ( $4.5 \times 10^{-12}$  N) of E7 at  $T_c - T = 5$  K. This value of  $W_0$  is comparable<sup>14,15</sup> to that reported in the literature for parallel anchoring on planar surfaces of treated glass substrates.<sup>16,17</sup> Using the above-mentioned rescaling of the elastic constants along with the proportionality  $K \propto S^2$ , the temperature dependence of  $W_0$  is obtained; it is presented in the inset of Fig. 1. There is a small hysteresis in this experiment which appears to not be more than 0.5 K. A very slow scanning rate,  $\sim 0.05$  K/min, is needed for determination of the configuration transition temperature.

If a uniform external field is applied, the free energies can again be calculated for the two nematic director configurations. The crossover free energies yield the points of transition for a droplet of radius  $R$  as a function of the field strength. Figure 2 shows the calculated regions of stability for the radial and axial configurations as a function of the ratio of extrapolation length to electric coherence length,  $d_e/\xi$ , where  $\xi = (K/\Delta\epsilon\epsilon_0)^{1/2}/E'$ . The figure shows that for small fields a droplet is either radial or axial according to the value of  $R/d_e$  relative to 18.2, as mentioned before. For very large fields all droplets will have the axial structure. There is a maximum field for which a radial droplet will exist. The radius of the droplet at this maximum field can be used to estimate the anchoring strength at the droplet surface. This

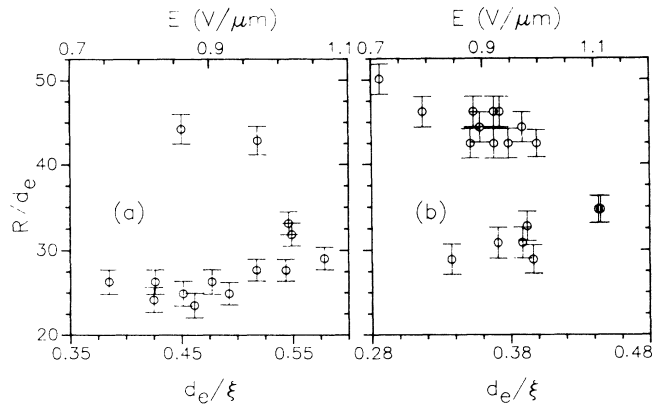


FIG. 3. Points of transition for the radial to axial configuration transition for droplets of different sizes in the presence of an external electric field  $E$  at  $T=298$  K for samples with E7, part A, and part B of TU50A mixed in a weight ratio of (a) 0.94:1:1.01 and (b) 0.99:1:1.10.

estimation is independent of the actual field needed to induce the transition. The radius described here is  $\sim 4 \mu\text{m}$  for this sample which at  $T_c - T = 5$  K yields a surface anchoring strength of  $\sim 3.9 \times 10^{-5} \text{ J/m}^2$ . This is approximately the same value as that calculated from the data in Fig. 1. Figure 3 shows the points of transition from radial to axial for this sample, and another with  $B/A = 1.10$ , as the strength of an external electric field is increased. The electric field was created by applying a 1-kHz ac voltage across the 25- $\mu\text{m}$ -thick samples. The magnitude of the electric field is plotted on the upper horizontal axis. The data in Fig. 3 have been rescaled to dimensionless parameters for comparison with Fig. 2 and are plotted along the lower horizontal axis. The material constants used to calculate the coherence length were  $K = 4.5 \times 10^{-12} \text{ N}$  and  $\Delta\epsilon = 7.3\epsilon_0$ . A reduction of approximately 0.2  $\text{V}/\mu\text{m}$  in the field strength for the transition was measured when the field was being decreased. This corresponds to a reduction of 0.01 in the parameter  $d_e/\xi$  as well.

The difference between the values of  $d_e/\xi$  in Fig. 3 and those calculated in Fig. 2 can be used to determine the local field within the droplet. Reducing the value of the applied field  $E$  (shown in Fig. 3) by factors of 7.4 for  $B/A = 1.01$  and 5.7 for  $B/A = 1.10$  will match the data to the theory. The local field  $E'$  is reduced because of the dielectric and resistive properties of the materials involved. An isolated droplet of isotropic material suspended in a polymer with dielectric constants  $\epsilon_{lc}$  and  $\epsilon_p$ , respectively, will have  $E' = 3E/(\epsilon_{lc}/\epsilon_p + 2)$ . The dielectric constant for materials with nonzero conductivities can be written as  $\epsilon = \epsilon' + j/\rho\omega$ , where  $\epsilon'$  is the dielectric permittivity,  $\rho$  is the resistivity, and  $\omega$  is the frequency of an applied ac voltage. In the dc limit ( $\epsilon'\epsilon_0\rho\omega \ll 1$ ), for materials with low resistivities, the resistive nature dominates, yielding the expression  $E' = 3E/(\rho_p/\rho_{lc} + 2)$ ,

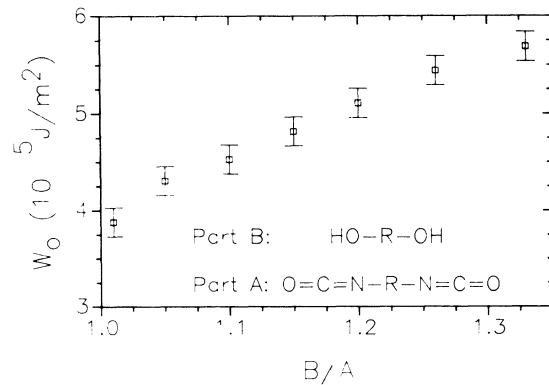


FIG. 4. Surface anchoring strengths at  $T=298$  K for samples with 32% E7 and 68% TU50A by weight, where the relative weights of parts A and B were varied.

where  $\rho_p$  and  $\rho_{lc}$  are the resistivities of the polymer binder and droplet material, respectively. The samples in this study have  $\rho_p \sim 10^9 \Omega \text{ cm}$ , yielding  $\epsilon'\epsilon_0\rho\omega \sim 10^{-1}$ . We are in the resistive regime and values of 20 ( $B/A = 1.01$ ) and 15 ( $B/A = 1.10$ ) for  $\rho_p/\rho_{lc}$  will account for the reduced local field.

Data like those shown in Fig. 3 were obtained for several samples with different values of  $B/A$  up to 1.33. The corresponding surface anchoring strengths are shown in Fig. 4. When  $B/A > 1.4$  the droplet diameter was larger than the spacing between the substrates. The relationship between droplet size and cure kinetics is discussed in Ref. 18.

It is demonstrated that the director configuration depends upon droplet size as well as on the orientation and strength of molecular anchoring at the droplet wall. External fields and temperature changes can be used to induce transitions in the director configuration, and these transitions can also be used to obtain a measure of the surface anchoring strength,  $W_0$ . It is interesting that perpendicular anchoring is achieved only when there is an excess of OH-R-OH (part B), indicating that it is necessary for some chains to terminate with OH groups for this condition. An increase in OH terminal groups is shown to increase the anchoring energy for perpendicular ordering.

An explanation of the need for larger applied electric fields to induce the radial-to-axial transition is given based on the resistivity ratio for the materials used. Because the droplets are formed from phase-separation processes, the ionic content of the droplet and matrix is probably similar; however, the mobility of the ions in the plastic matrix is no doubt lower, increasing the resistivity of the matrix over that of the droplet. The ratio  $\rho_p/\rho_{lc} \approx 20$  is not an unreasonable value and a plausible explanation to the reduced value of the electric field inside the droplet. The experiment presented here can be used as a way of studying the differences between the applied electric field and the local electric field within the drop-

let. Experiments are under way for the use of magnetic fields to check this point. More experiments on different types of PDLC's are planned, as well as studies of the effects of droplet shape on director configurations and configuration transitions.

As mentioned earlier, the surface contributions of the saddle-splay term and the mixed splay-bend term were neglected in Eq. (1) because of the lack of information about the  $K_{13}$  and  $K_{24}$  elastic constants.<sup>19</sup> Theoretical calculations including different values for all elastic constants and the previously omitted surface contributions are in progress. The resulting phase diagrams have qualitatively the same shape, but scales may differ by a factor of 2 depending upon the values of the elastic constants.

The authors acknowledge valuable discussions with the PDLC groups at General Motors Research Laboratories and Hughes Research Laboratories. The research was supported in part by the National Science Foundation under Solid State Chemistry Grant No. DMR88-17647.

---

<sup>(a)</sup>Permanent address: Department of Physics, E. Kardelj University of Ljubljana, Jadranska 19, 61000, Ljubljana, Yugoslavia.

<sup>1</sup>E. Dubois-Violette and O. Parodi, *J. Phys. (Paris), Colloq.* **30**, C4-57 (1969).

<sup>2</sup>M. J. Press and A. S. Arrot, *Phys. Rev. Lett.* **33**, 403

(1974).

<sup>3</sup>S. Candau, P. LeRoy, and F. Debeauvais, *Mol. Cryst. Liq. Cryst.* **23**, 283 (1973).

<sup>4</sup>S. Žumer and J. W. Doane, *Phys. Rev. A* **34**, 3373 (1986).

<sup>5</sup>R. D. J. Williams, *J. Phys. A* **19**, 3211 (1986).

<sup>6</sup>G. E. Volovik and O. D. Laurentovich, *Zh. Eksp. Teor. Fiz.* **85**, 1997 (1983) [*Sov. Phys. JETP* **58**, 1159 (1983)].

<sup>7</sup>P. Drzaic, *Mol. Cryst. Liq. Cryst.* **154**, 289 (1987).

<sup>8</sup>A. Poniewierski and T. J. Sluckin, *Liq. Cryst.* **2**, 281 (1987).

<sup>9</sup>A. Golemme, S. Žumer, D. W. Allender, and J. W. Doane, *Phys. Rev. Lett.* **61**, 2937 (1988).

<sup>10</sup>D. W. Allender and S. Žumer, *Proc. SPIE Int. Soc. Opt. Eng.* **1080**, 18 (1989).

<sup>11</sup>P. Sheng, *Phys. Rev. Lett.* **37**, 1059 (1976); *Phys. Rev. A* **26**, 1610 (1982).

<sup>12</sup>J. W. Doane, A. Golemme, J. L. West, J. B. Whitehead, Jr., and B.-G. Wu, *Mol. Cryst. Liq. Cryst.* **165**, 511 (1988).

<sup>13</sup>P. G. de Gennes, *Mol. Cryst. Liq. Cryst.* **12**, 193 (1972).

<sup>14</sup>L. G. Grechkno, T. Ya. Marsuii, Yu. A. Reznikov, and A. I. Khizhnyak, *Ukr. Fiz. Zh.* **32**, 1213 (1987).

<sup>15</sup>G. W. Smith, N. A. Vaz, and T. H. VanSteenkiste (to be published).

<sup>16</sup>H. Yokoyama and H. A. van Sprang, *J. Appl. Phys.* **57**, 4520 (1985).

<sup>17</sup>J. T. Gleeson and P. Palfy-Muhoray, *Liq. Cryst.* **5**, 663 (1989).

<sup>18</sup>G. W. Smith and N. A. Vaz, *Liq. Cryst.* **3**, 543 (1988).

<sup>19</sup>A. Strigazzi, *Nuovo Cimento* **10**, 1335 (1988); *Mol. Cryst. Liq. Cryst.* **152**, 435 (1987).